SANDIA REPORT
SAND2009-6419
Unlimited Release
Printed September 2009

Tuned Cavity Magnetometer

Murat Okandan, Peter Schwindt

Prepared by
Sandia National Laboratories
Albuquerque, New Mexico 87185 and Livermore, California 94550

Sandia is a multiprogram laboratory operated by Sandia Corporation,
a Lockheed Martin Company, for the United States Department of Energy's
National Nuclear Security Administration under Contract DE-AC04-94AL85000.

Approved for public release; further dissemination unlimited.

Sandia National Laboratories

Issued by Sandia National Laboratories, operated for the United States Department of Energy by Sandia Corporation.

NOTICE: This report was prepared as an account of work sponsored by an agency of the United States Government. Neither the United States Government, nor any agency thereof, nor any of their employees, nor any of their contractors, subcontractors, or their employees, make any warranty, express or implied, or assume any legal liability or responsibility for the accuracy, completeness, or usefulness of any information, apparatus, product, or process disclosed, or represent that its use would not infringe privately owned rights. Reference herein to any specific commercial product, process, or service by trade name, trademark, manufacturer, or otherwise, does not necessarily constitute or imply its endorsement, recommendation, or favoring by the United States Government, any agency thereof, or any of their contractors or subcontractors. The views and opinions expressed herein do not necessarily state or reflect those of the United States Government, any agency thereof, or any of their contractors.

Printed in the United States of America. This report has been reproduced directly from the best available copy.

Available to DOE and DOE contractors from
U.S. Department of Energy
Office of Scientific and Technical Information
P.O. Box 62
Oak Ridge, TN 37831

Telephone: (865) 576-8401
Facsimile: (865) 576-5728
E-Mail: reports@adonis.osti.gov
Online ordering: http://www.osti.gov/bridge

Available to the public from
U.S. Department of Commerce
National Technical Information Service
5285 Port Royal Rd.
Springfield, VA 22161

Telephone: (800) 553-6847
Facsimile: (703) 605-6900
E-Mail: orders@ntis.fedworld.gov
Online order: http://www.ntis.gov/help/ordermethods.asp?loc=7-4-0#online

SAND2009-6419
Unlimited Release
Printed September 2009

Tuned Cavity Magnetometer

Murat Okandan, Peter Schwindt

Sandia National Laboratories
P.O. Box 5800
Albuquerque, New Mexico 87185-MS1080

Abstract

We have developed a high sensitivity (<picoTesla/√Hz), non-cryogenic magnetometer that utilizes a novel optical (interferometric) detection technique. Further miniaturization and low-power operation are key advantages of this magnetometer, when compared to systems using SQUIDs which require liquid Helium temperatures and associated overhead to achieve similar sensitivity levels.

CONTENTS

1. Introduction 7
   1.1. Experimental setup 9
2. Fabrication 11
   2.1 Microfabricated components 11
   2.2 Meso-scale fabricated components 12
3. Measurements 15
   3.1 Baseline Faraday Rotation Magnetometer 15
   3.2 First MEMS Tunable Mirror 16
   3.3 Piezo Actuated Gold on Glass Mirror 17
   3.3 Second MEMS Tunable Mirror 19
4. Conclusions 21
Distribution 22

FIGURES

Figure 1. Basic elements of an atomic magnetometer. A glass cell contains an alkali vapor. A circularly polarized pump laser beam aligns the electron spins. The collective spin precesses around an external magnetic field. A pump beam detects the precession of the atomic polarization. 8
Figure 2. (a) Measurement setup and beam paths for pump/probe and displacement detection of the mirror and cavity size. (b) Model of boron nitride holder with other components inserted. (c) Cs vapor cell. (d) Magnetic shields with holder and field coils installed. 10
Figure 3. Reflector design 1 (RS620) and fabricated device. 11
Figure 4. Reflector devices mounted on ceramic holder with heaters and thermistor. 11
Figure 5. SOI based reflector design and fabricated device (RS772). 12
Figure 6. Solidworks model and the fabricated boron nitride holder on teflon base with mirror mounts. 12
Figure 7. (a) Double layer magnetic shields and field coils. (b) Endcaps installed with openings for optical access of pump/probe beams. (c) Boron nitride holder inserted into position with the teflon base. 13
Figure 8. LTCC holders with alignment features, heaters, thermistor and electrical connection pads for the reflector device. 14
Figure 9. Gold on quartz diffractions gratings with various pitch and duty cycle variations. 14
Figure 10. Output of the balanced polarimeter as the vertical magnetic field is swept. The width of the magnetic resonance is 47 nT corresponding to 165 Hz. 15
Figure 11. (a) The normalized frequency response of the SERF magnetometer using the conventional Faraday rotation detection. (b) The sensitivity of the SERF magnetometer as a function of frequency. Noise of the magnetometer measured directly from the photodiode signal (black line). Magnetometer noise scaled by the frequency response representing the sensitivity of the magnetometer (red line). The photon shot noise limit scaled by the frequency response (blue line). 15

Figure 12. The left plot shows the magnetic sensitivity of the interferometric technique using a MEMS mirror and a grating (black) compared to the Faraday detection technique (red). The right plot shows the voltage noise output from the lock-in amplifier under different conditions. The optical noise is taken when the pump beam is blocked eliminating any sensitivity to magnetic fields. The fact that the magnetometer noise (black) is equivalent to the optical noise (red) shows that the noise in the system is due to sensing technique. The electronic noise (blue) is measured when no light is on the photodetector. The green line shows the photon shot noise. 16
Figure 13. (a) A comparison of the sensitivity of the three optical setups. (b) The normalized frequency response of the interferometric technique. (c) Data from the interferometric technique showing the noise of the magnetometer, the optical noise, the electronic noise, and the shot noise (straight blue line). (d) Data from the Faraday technique with the same optical setup showing the noise of the magnetometer, the optical noise, the electronic noise, and the shot noise (straight blue line). 18

1. INTRODUCTION

By use of the techniques of microelectromechanical systems (MEMS) and small efficient semiconductor diode lasers, alkali atom vapor cell based devices have recently been drastically miniaturized with corresponding reductions in power consumption. Devices such as atomic clocks, atom-optical magnetometers, and nuclear magnetic resonance gyroscopes have all been miniaturized to a remarkable degree while their performance has been minimally degraded. The miniaturization of the atomic magnetometers has lead to interesting applications such as compact, low-field magnetic resonance imaging. Fully integrated miniaturized atomic magnetometers operate in the Earth's field regime (1-100 μT), and their sensitivities have been limited to > 2 pT $Hz^{-1/2}$. As recently demonstrated, the sensitivity of atomic magnetometers can be drastically reduced by operating in the low-field, spin-exchange relaxation-free (SERF) regime, and when implemented in a miniaturized vapor cell, a sensitivity of 70 fT $Hz^{-1/2}$ was demonstrated. This magnetometer was implemented with a single laser beam both to optically pump the atoms and to probe their response to a magnetic field. In general, the sensitivity of an atomic magnetometer can be improved by separating the pump and probe beams so the parameters of the beams can be optimized independently. In this work, we demonstrate an interferometric technique for implementing a probe beam that is readily integrated into a miniaturized device and lends itself to lock-in detection for improved noise rejection.

SERF magnetometers are traditionally implemented by directing a pump laser and a probe laser such that they propagate perpendicular to each other and intersect in the center of an alkali vapor cell. The pump laser is circularly polarized and optically pumps the spins of the alkali atoms along the propagation direction of the beam. Because the magnetometer is operated near zero field, the Larmor spin precession frequency is much smaller than the spin decoherence rate, and a large atomic polarization, P_z, is generated. In addition, the Larmor frequency is much smaller than the spin exchange rate, and spin exchange is no longer a source of decoherence. Eliminating spin exchange reduces the decoherence rate by two to three orders of magnitude, thereby improving the sensitivity of the SERF magnetometer by a similar amount. The SERF magnetometer is to first order sensitive to fields along the y-direction, B_y. When a small magnetic field is applied, the spins precess about the field and a small component of the atomic polarization is generated in the x-direction. The amount of atom polarization, P_x, is proportional to magnetic field B_y. The x-component of the atomic polarization is traditionally measured with an off-resonant, linearly polarized probe beam, and due to the Faraday Effect, the linear polarization is rotated by an amount proportional to the atomic polarization. Polarization rotation arises because the left circularly polarized light accumulates a phase shift different from right circularly polarized light as it propagates through the atomic medium.

The technique that is used in this project measures P_x with a variant of a Michelson interferometer. The interferometer measures the phase shift of a circularly polarized, off-resonant probe beam as it passes though the vapor cell. The index of refraction of the atomic medium and thereby the accumulated phase depend on the atomic polarization as

$$\varphi_{\pm} = \frac{2l\omega}{c}\left(1 + \frac{2\pi n c^2 r_e f}{\omega} D(\omega) \frac{1 \mp P_x}{2}\right)$$

where l is the length of the cell, ω is the frequency of the light, c is the speed of light, n is the

$$D(\omega) = \frac{\omega - \omega_0}{(\omega - \omega_0)^2 + (\gamma/2)^2}$$

number density of the alkali atoms, r_e is the classical electron radius, f is the oscillator strength. The ± refers to right or left circular polarization. The dispersive lineshape function is given by where, ω_0 is the resonant frequency of the optical transition and γ is the width of the optical transition. Forming the interferometer is a diffraction grating on one side of the cell and a MEMS fabricated tunable mirror on the other. The grating is made by lithographically pattering gold lines on glass. The grating both transmits light to vapor cell and reflects light into the zero, first, and higher order modes. The transmitted light travels through the vapor cell, reflects off the tunable mirror, and travels back to the grating. Interference occurs between the light reflected from the grating and the transmitted light such that when constructive interference is observed in the zero order reflected beam, destructive interference is observed in the first order modes. The tunable mirror allows the optical path length to be adjusted with picometer resolution and the interferometer to be tuned to achieve maximum response to changes in index of refraction.

The interferometric approach to implementing the probe beam offers several advantages when miniaturizing a SERF magnetometer. The main technique for implementing lock-in detection when measuring Faraday rotation is to modulate the polarization angle. This is typically implemented with either a Faraday modulator where a large oscillating magnetic field is applied to a material with a large Verdet constant or a photoelastic modulator where a material is periodically squeezed to modulate its birefringence. Both techniques are difficult to integrate

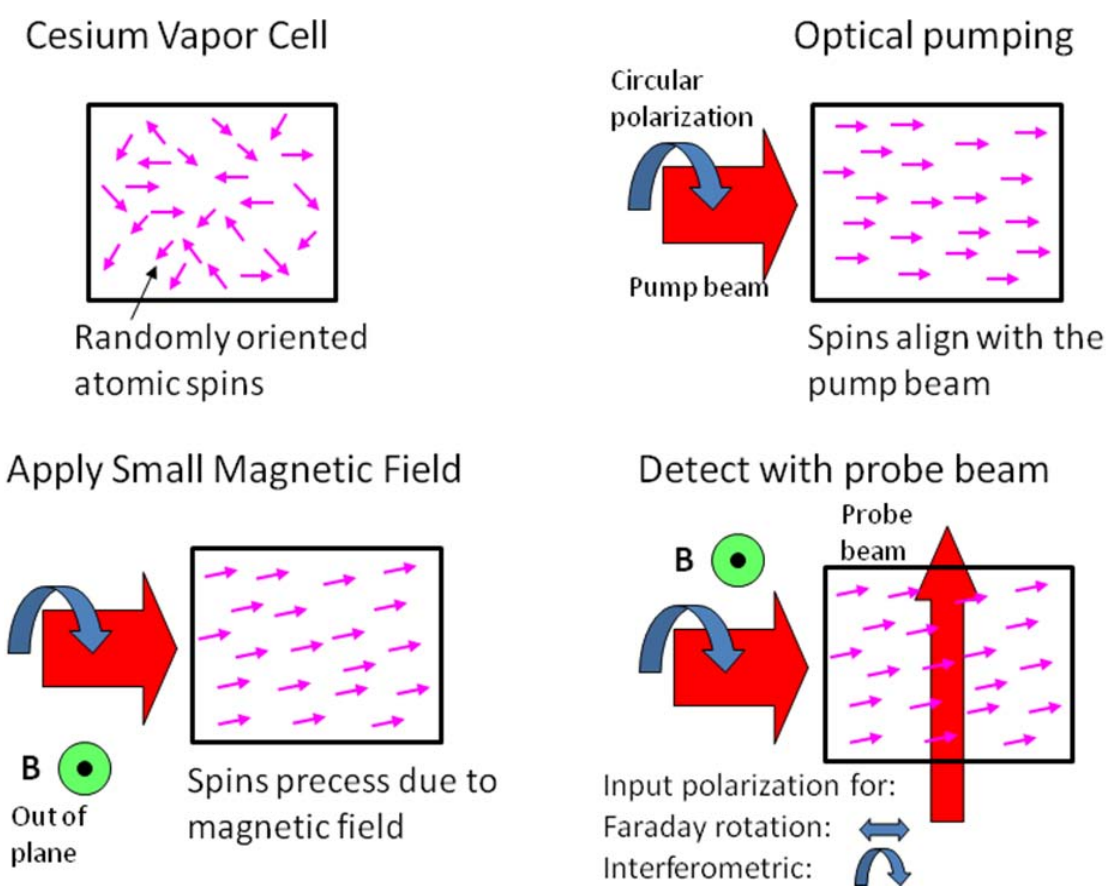

Figure 1. Basic elements of an atomic magnetometer. A glass cell contains an alkali vapor. A circularly polarized pump laser beam aligns the electron spins. The collective spin precesses around an external magnetic field. A pump beam detects the precession of the atomic polarization.

into a device millimeters in size. On the other hand, the MEMS tunable mirror is readily modulated at several kHz allowing lock-in detection. The largest dimension of the mirror is 4 mm and could easily be made smaller. In fact, fully integrated accelerometers and microphones using the same interferometric detection scheme have already been implemented.

1.1. Experimental setup

The experimental setup for the device is shown in Fig. 2. A vapor cell contains the Cs vapor and buffer gases. The interior dimensions of the cell are $4 \times 4 \times 10$ mm^3 plus a tip off tube. The estimated buffer gas pressure is 450 Torr of Ne and 30 Torr of N_2. The buffer gas homogeneously broadens the optical absorption lines to 5 GHz such that the excited state hyperfine structure is not resolved but the ground state structure is. The cell is heated to 100 °C by passing 100 kHz alternating current through a low temperature co-fired ceramic heater. The heaters are of the same dimensions as the face of the cell, and a heater is placed on faces of the cell where the pump laser passes through. The electrical traces in the ceramic heater are laid out to minimize the field produced by the currents passing through the conductors. Two distributed feedback (DFB) lasers are used to optically pump and probe the Cs vapor cell. The lasers are tuned near the D1 line of Cs at 895 nm. The pump laser is circularly polarized and tuned to be resonant with the transition from the $^2S_{1/2}$ $F = 4$ ground state to the $^2P_{1/2}$ excited state. The probe laser propagates perpendicular to the pump beam and is detuned to the red of the $F = 4$ transition by several gigahertz. Depending on whether we are using the traditional Faraday detection or detecting the index of refraction of the Cs vapor, the polarization of the probe laser is linear or circular, respectively. The cell is contained within a two-layer cylindrical magnetic shield where the inner shield is 15.2 cm in diameter and 30.5 cm long, and coils within the shield allow control of the magnetic field along all three directions. A 1.5 cm × 14.2 cm slot is cut in one of the end caps to allow varying angles of the diffracted probe beam to exit the shield.

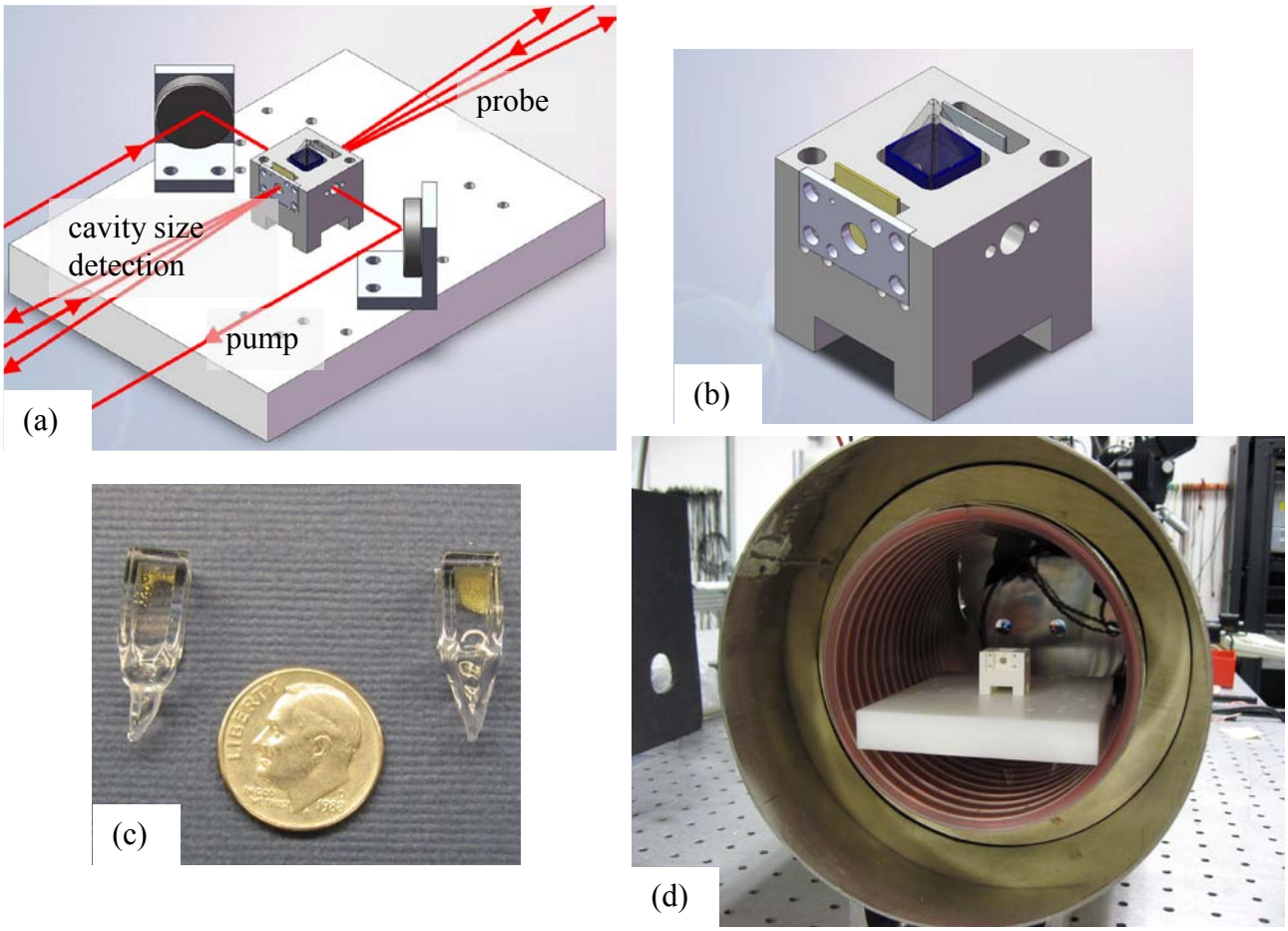

Figure 2. (a) Measurement setup and beam paths for pump/probe and displacement detection of the mirror and cavity size. (b) Model of boron nitride holder with other components inserted. (c) Cs vapor cell. (d) Magnetic shields with holder and field coils installed.

2. FABRICATION

2.1 Microfabricated components

Several different micro-scale components were fabricated and integrated in the magnetometer setup. Three different reflector structures were designed and fabricated using surface micromachining and DRIE to provide the required optical access through the silicon substrate. AutoCAD mask views and images of the various designs are shown below.

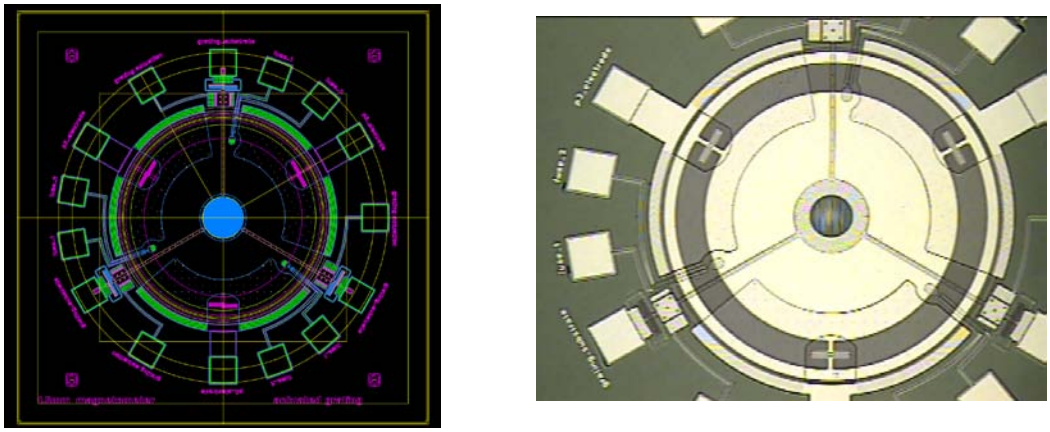

Figure 3. Reflector design 1 (RS620) and fabricated device.

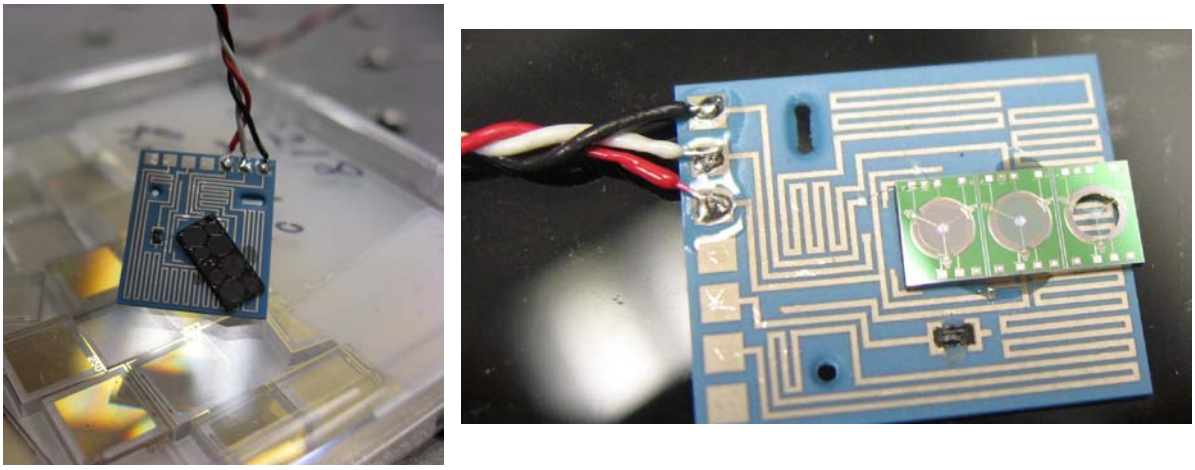

Figure 4. Reflector devices mounted on ceramic holder with heaters and thermistor.

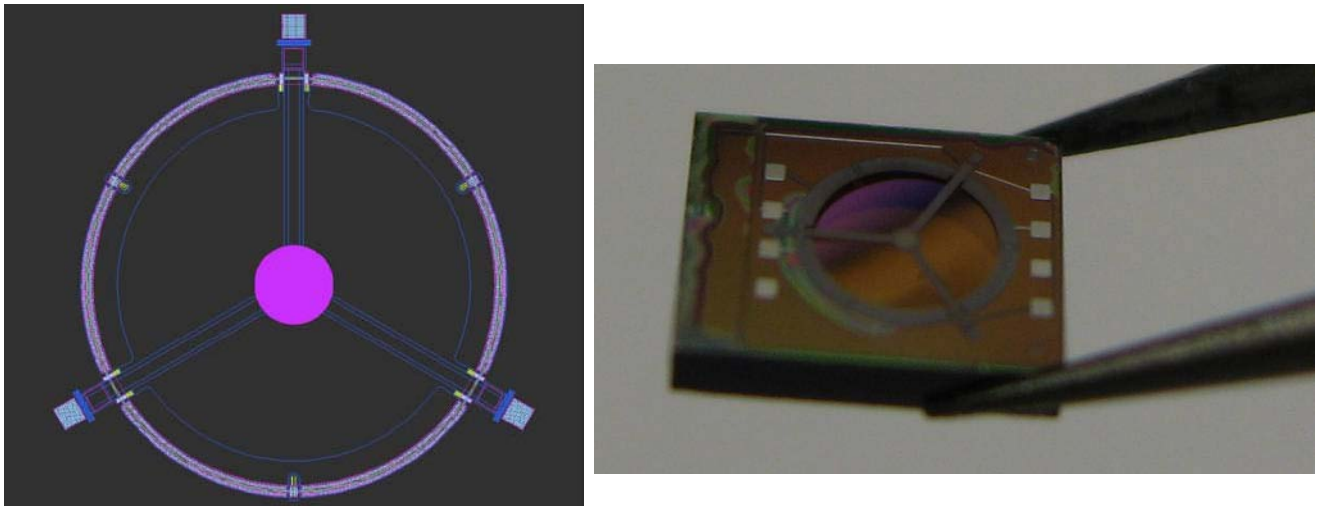

Figure 5. SOI based reflector design and fabricated device (RS772).

2.2 Meso-scale fabricated components

Other meso-scale machined components were used to assemble these components together. A boron nitride holder was designed and fabricated to provide minimal mechanical expansion due to temperature changes (Figure 6).

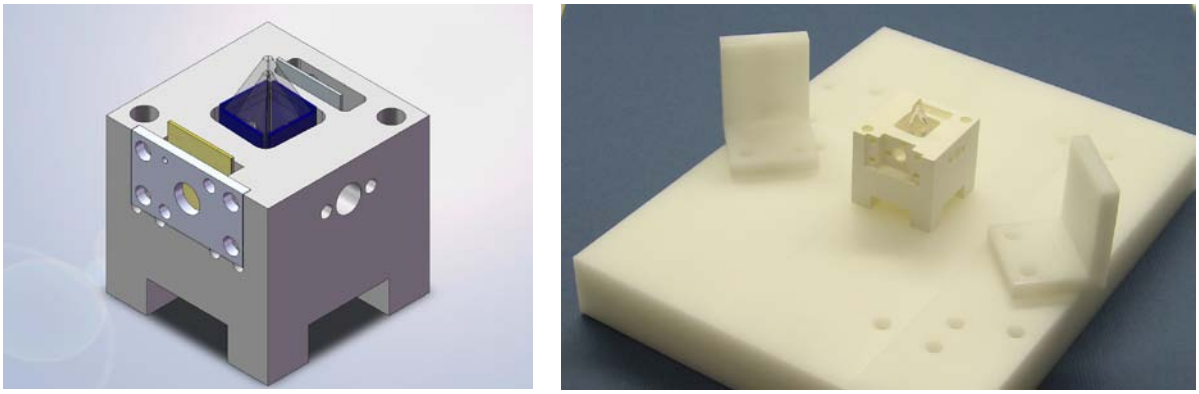

Figure 6. Solidworks model and the fabricated boron nitride holder on teflon base with mirror mounts.

Magnetic shields are necessary to provide the near-zero magnetic field for the operation of the magnetometer. In addition field coils were also fabricated and inserted inside the shield to null-out the remaining magnetic fields and apply known test signals (Figure 7).

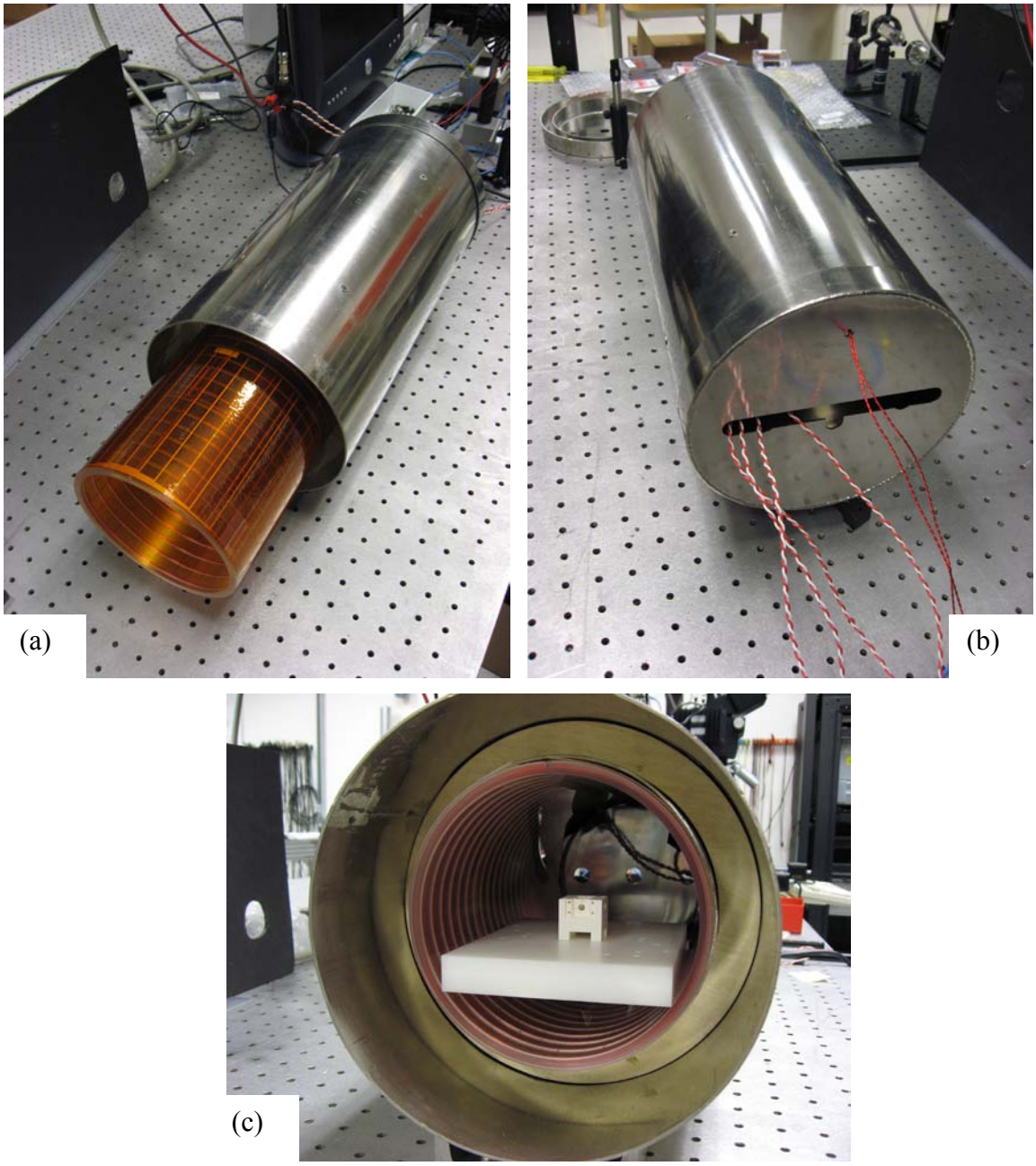

Figure 7. (a) Double layer magnetic shields and field coils. (b) Endcaps installed with openings for optical access of pump/probe beams. (c) Boron nitride holder inserted into position with the teflon base.

Low-temperature co-fired ceramic (LTCC) holders were designed to accommodate individual components such as the reflector and also to provide the required heating for increasing the alkali atom vapor density inside the vapor cell. The holders had mechanical alignment features that matched to the tilt adjustment components of the boron nitride holder.

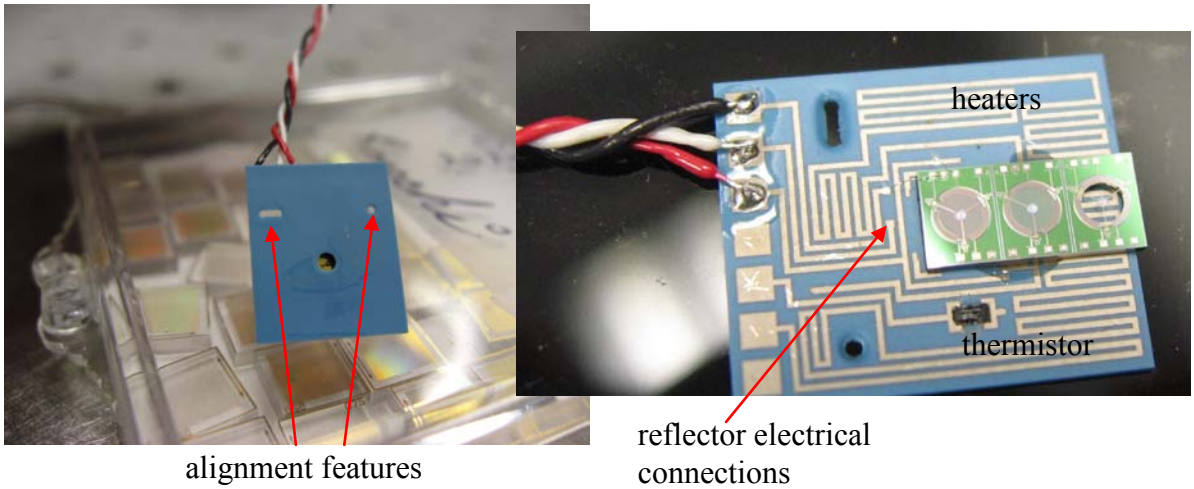

Figure 8. LTCC holders with alignment features, heaters, thermistor and electrical connection pads for the reflector device.

Diffraction gratings with a 5 micron pitch and various duty cycles were fabricated using aluminum on quartz and gold on quartz. These components are placed in the probe beam-path, in front of the vapor cell containing the alkali atoms, forming the first interface of the tuned cavity.

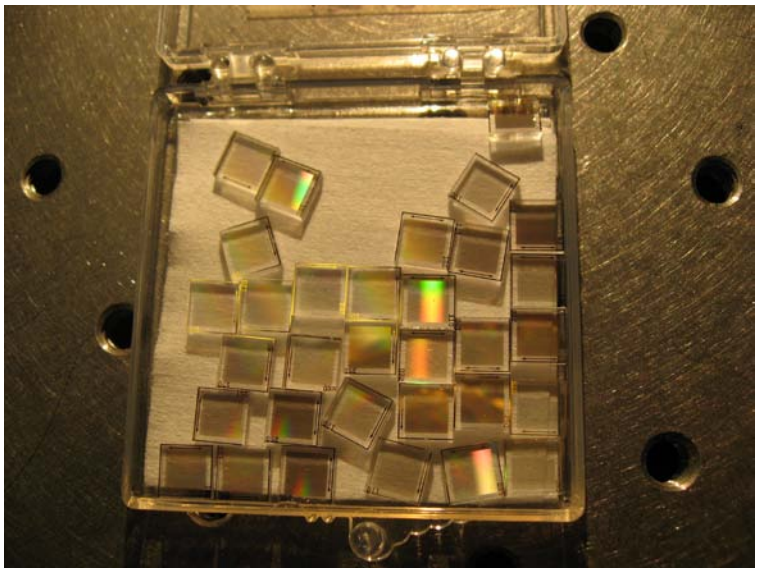

Figure 9. Gold on quartz diffractions gratings with various pitch and duty cycle variations.

3. MEASUREMENTS

3.1 Baseline Faraday Rotation Magnetometer

Our first measurement effort was focused on characterizing the performance of a standard Faraday rotation SERF magnetometer. The goal of these measurement is to understand the limits of the magnetometer and to indentify the major noise sources in the system. For this magnetometer the probe beam light was linearly polarized and simply passed straight through the vapor cell to a balanced polarimeter. The balance polarimeter has a polarizing beam splitter oriented at 45° to the probe beam polarization. The two beams are sent to a photodetector that subtracts the intensity of the two beams. A nonzero output of the photodetector represents a rotation of the polarization of the probe beam.

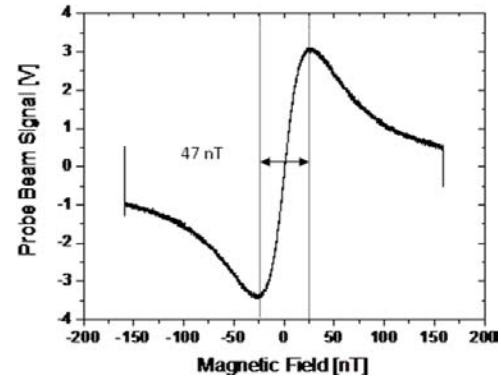

Figure 10. Output of the balanced polarimeter as the vertical magnetic field is swept. The width of the magnetic resonance is 47 nT corresponding to 165 Hz.

The magnetometer signal is shown in Figure 11 as the magnetic perpendicular to the plane formed by the pump and the probe beam is swept. To measure the noise of the magnetometer, the magnetic field is set to the zero where the slope of the atomic response to the magnetic field is the steepest and approximately linear. The voltage noise from the balance polarimeter is sent to a spectrum analyzer where the voltage noise

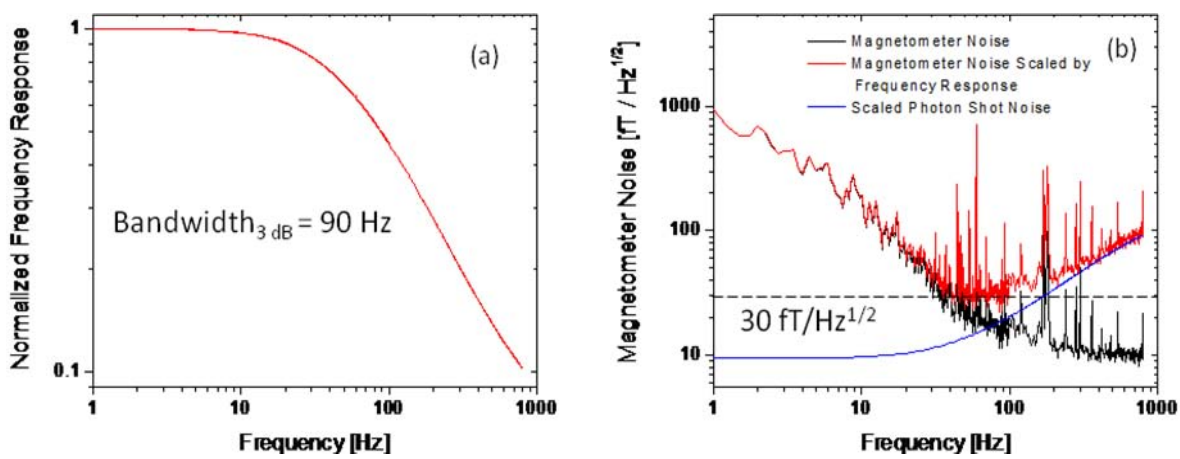

Figure 11. (a) The normalized frequency response of the SERF magnetometer using the conventional Faraday rotation detection. (b) The sensitivity of the SERF magnetometer as a function of frequency. Noise of the magnetometer measured directly from the photodiode signal (black line). Magnetometer noise scaled by the frequency response representing the sensitivity of the magnetometer (red line). The photon shot noise limit scaled by the frequency response (blue line).

density is recorded. This noise is divided by the slope of the signal to convert to units of magnetic noise density (Figure 11(b)). The magnetometer has a finite frequency response, which can be measured by sending a chirped frequency sine wave to modulate the magnetic field. The recorded response is shown in Figure 11(a) demonstrating a bandwith of 90 Hz. The sensitivity of the magnetometer is given by dividing the magnetometer noise by the frequency response. The best sensitivity of 30 fT/Hz$^{1/2}$ is seen in the range of 30-100 Hz. At higher frequencies the sensitivity is limited the frequency response of the magnetometer and approaches the photon shot noise limit. At lower frequencies $1/f$ noise begins to dominate. This is often attributed to air currents causing beam pointing instabilities although this was not explicitly verified for this experiment. For these measurements, the intensities of the pump and probes beams were 4.2 mW/cm^2 and 1.8 mW/cm^2 respectively. The pump beam was tuned to be resonant with the F = 4 ground state to the excited state transition and the probe beam was detuned by 8.9 GHz to the red of this transition. The temperature of the cell was 100° C.

3.2 First MEMS Tunable Mirror

The first interferometric measurements made with a MEMS tunable mirror where performed with prototype reflector structures originally designed as a microphone. Because this device was not designed for magnetometery, the Si mirror could not be gold coated. This reduced the reflectivity to ~ 30%. The grating that was used was aluminum on fused silica with a 5 μm pitch and a 30% duty cycle. The reduced duty cycle allows greater transmission through the grating. This balances the fact that there is more loss in the transmitted beam than the reflected beam, thereby increasing the fringe visibility of the interferometer.

The tunable mirror and the grating have to be perfectly parallel to achieve high visibility interference fringes, and several factors made this difficult to achieve. The mount for the tunable

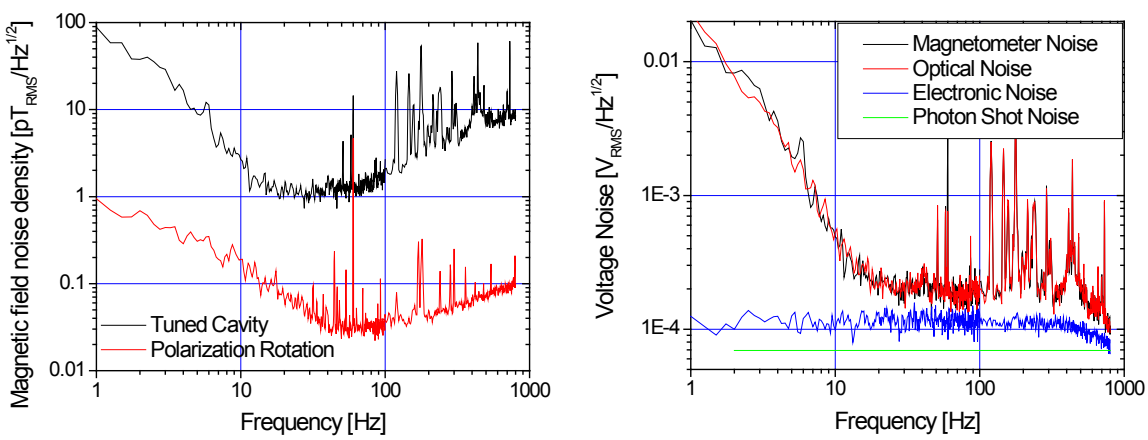

Figure 12. The left plot shows the magnetic sensitivity of the interferometric technique using a MEMS mirror and a grating (black) compared to the Faraday detection technique (red). The right plot shows the voltage noise output from the lock-in amplifier under different conditions. The optical noise is taken when the pump beam is blocked eliminating any sensitivity to magnetic fields. The fact that the magnetometer noise (black) is equivalent to the optical noise (red) shows that the noise in the system is due to sensing technique. The electronic noise (blue) is measured when no light is on the photodetector. The green line shows the photon shot noise.

mirror was not very robust, and the alignment had to be performed outside the shield. When the interferometer/cell structure was moved into the shield the alignment could change. In addition, heating and cooling the cell would cause the alignment to shift. Due to small thickness of the Si mirror (2.5 μm), it was not flat and its shape would change with temperature. Also, the windows of the cell appear to be curved and wedged which has the effect of varying the optical path length across the diameter of the beam. The visibility observed was 12% on one the first order diffracted beams.

To measure the magnetic sensitivity with the interferometric technique, the mirror position is modulated at 10 kHz. The modulation also provides a reference to a lock-in amplifier. The amplitude of the modulation to the mirror is 2 V_{PP} with the DC offset that varies from 10-30 V. The first order beam is sent to the photodetector whose signal is demodulated with the lock-in amplifier. The length of the interferometer is tuned so that at zero magnetic field the interferometer signal is modulated about the peak of a fringe. At this point, the photodetector signal contains no signal at the modulation frequency, only at twice the modulation frequency, thereby setting the lock-in output to zero. When a change in optical path length occurs, from a magnetic field for example, the output from the lock-in linearly deviates from zero.

The measured magnetic field sensitivity with this setup is shown in Figure 12. The noise from this technique is substantially higher than the polarization rotation technique. There are several factors that contribute to degraded sensitivity: Length fluctuations are equivalent to changes in magnetic field so the device is more sensitive to vibration. Given our voltage noise level of 275 μV/Hz$^{1/2}$ at 20 Hz, the equivalent length change would be 23 pm/Hz$^{1/2}$. If our noise were attributable to changes in index of refraction, the equivalent change would be 1.4×10^{-9}/Hz$^{1/2}$. This could arise due to convection currents around the hot cell. Also, laser frequency noise is could be a significant noise source where the equivalent change would be 17 MHz/Hz$^{1/2}$. The laser noise had been previously estimated to be 11 MHz. In addition to these possible contributors to the noise, factors that contribute to reduced signal size mainly reduce the visibility of the interference fringes. These include the curved tunable mirror and cell walls and poor collimation of the probe laser.

3.3 Piezo Actuated Gold on Glass Mirror

In an effort to understand the noise and signal size issues associated with the interferometric technique, we removed the MEMS tunable mirror and replaced it with a gold coated microscope coverslip mounted on a miniature PZT 2× 2×2 mm^3 from Physik Instrumente, part number PL022.30. The gold coated glass was much flatter than the MEMS mirror and had a much greater reflectivity, presumably close to the ideal reflectivity of gold of > 95% but this was not measured. To further increase the signal size, the grating was replaced with one made with gold on a titanium adhesion layer on glass fabricated with a gold lift-off process. The duty cycle was 25%. The gold grating should perform better than the Al grating due to its greater reflectivity at 895 nm. In addition, the probe beam was passed through a single mode polarization maintaining fiber, improving the spatial mode of the beam. With these improvements we were able to increase the visibility to > 60% on the zero order beam and > 30% on the first order beam. However, this was when the interferometer/cell setup was outside the shield. When first installed in the shield, the visibility would be maintained for a short period of time and then degrade over several days as the alignment drifted. We also detected both the zero and first order beams on the balanced photodetector. Since interferometric signal for the zero and first order beams are 180°

out of phase, subtracting the signals increases signals while removing common mode noise, *e.g.* amplitude noise. The result of the increased signal size was to improve the sensitivity by roughly a factor of two.

In addition to improving the signal size, work also focused on reducing the noise from the interferometer. Laser frequency noise was identified as a significant noise source in the previous measurements so we switched to an external cavity diode laser that is specified to have a linewidth < 100 kHz. This laser was resonant with the D2 line of Cs at 852 nm. This improved the sensitivity by another factor of two. We also attempted to reduce noise associated with instabilities in the length of the interferometer. We drove the PZT with a low-noise battery source but this had little effect. We also attempted to stabilize the length of the interferometer by sending off-resonant light at 770 nm through the interferometer. The signal was fed back to the PZT through proportional and integral loop filter amplifier to provide active length stabilization. It was presumed this would significantly reduce the 1/f noise in the magnetometer signals, but it was unchanged when the feedback was applied.

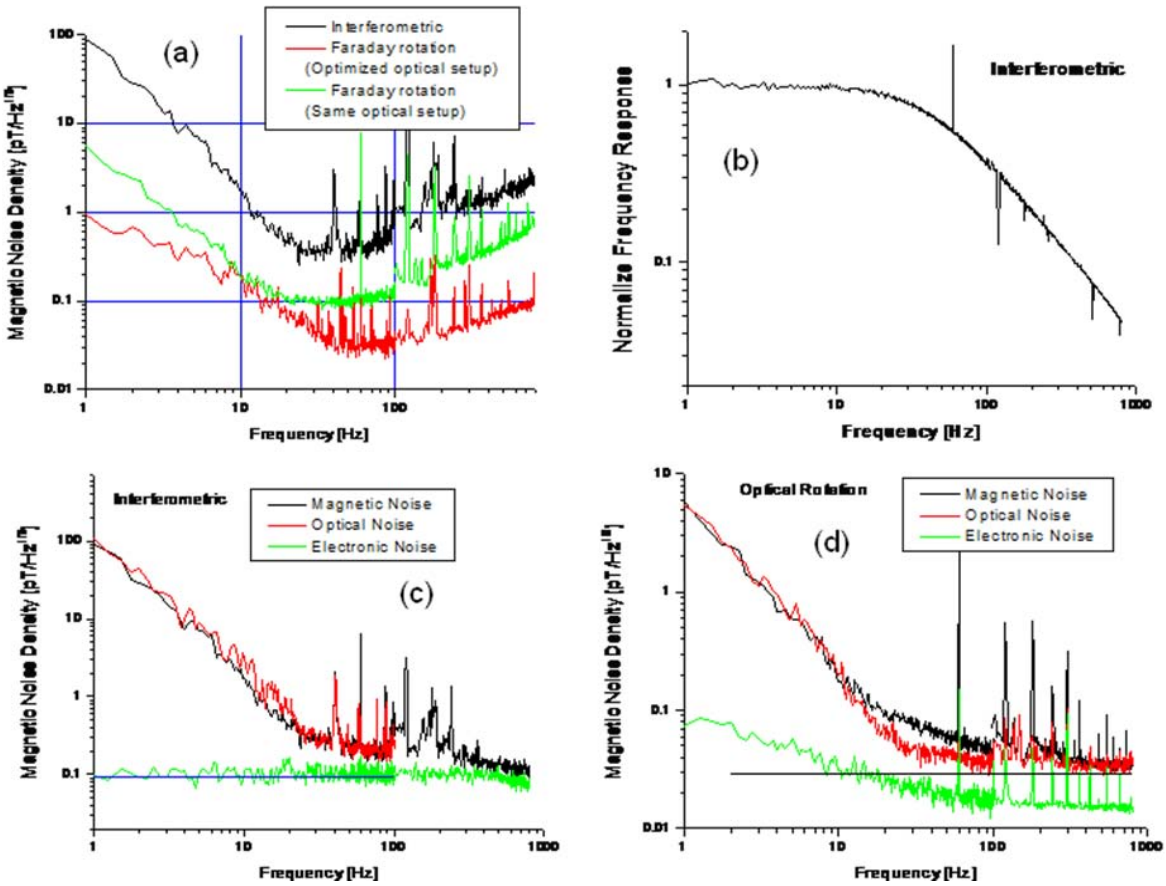

Figure 13. (a) A comparison of the sensitivity of the three optical setups. (b) The normalized frequency response of the interferometric technique. (c) Data from the interferometric technique showing the noise of the magnetometer, the optical noise, the electronic noise, and the shot noise (straight blue line). (d) Data from the Faraday technique with the same optical setup showing the noise of the magnetometer, the optical noise, the electronic noise, and the shot noise (straight blue line).

To make a fair comparison between the interfeterometric approach and the Faraday rotation approach, measurements of Faraday approach were taken using the same optical path as the interferometer but with the grating removed. A comparison of the techniques is shown in Figure 13.

3.3 Second MEMS Tunable Mirror

Next we installed the another MEMS tunable mirror. Even though this mirror was designed for a microphone application is could be gold coated giving much higher reflectivity. The curvature of the mirror reduced the visibility to a maximum of 15% on the zero order and 7% on the first order, and the visibility degraded over time. Even with the improved reflectivity of the mirror, the visibility was reduced by nearly a factor of two compared to our first MEMS tunable mirror which had a visibility of 12% on the first order beam. In the current case we did detect both zero and first order beams. The end result was that the sensitivity of the two MEMS mirror setups where equivalent at 1 $pT/Hz^{1/2}$. Interestingly, other noise sources dominated over the laser frequency noise, and the noise level was independent of the laser used.

4. CONCLUSIONS

We have designed and assembled a high sensitivity (<picoTesla/√Hz) miniaturized atomic magnetometer which does not require cryogenic cooling. Further miniaturization of this device and measurement technique is also possible. We have considered integration of polarization detectors, fiber based beam delivery for lower volume and evacuation of the measurement chamber for achieving further improvement of sensitivity levels and reduction of noise in the system.

While the ultimate sensitivity level achieved by macro-scale atomic magnetometers (<femtoTesla/√Hz) was not observed in this miniaturized device, we have demonstrated the initial feasibility of this approach and have pathways available for approaching the theoretical limits of sensitivity that is possible. For many of the applications that require a fieldable system, the demonstrated sensitivity level is more than adequate (approximately an order of magnitude lower than other approaches).

Further integration with other sensor platforms and low logistical overhead (compared to cryogenic support systems) are expected to lead to novel applications in areas such as geophysical sensing, navigation, underground/underwater structure mapping and medical diagnostics (ultra-low field MRI/MEG, neural current mapping).

DISTRIBUTION

1	MS1080	Murat Okandan	01749
1	MS1082	Peter Schwindt	01725
2	MS9018	Central Technical Files	8944
2	MS0899	Technical Library	4536
1	MS0123	D. Chavez, LDRD Office	1011

Sandia National Laboratories